Simulating cancer-cell kinetics after drug treatment: Application to cisplatin on ovarian carcinoma

F. Montalenti
Istituto di Ricerche Farmacologiche ''Mario Negri,'' 20157 Milano, Italy
and Istituto Nazionale di Fisica della Materia (INFM), Università di Genova, Dipartimento di Fisica, Via Dodecaneso 33, 16146 Genova, Italy

G. Sena*
Istituto di Ricerche Farmacologiche ''Mario Negri,'' 20157 Milano, Italy

P. Cappella and P. Ubezio
Istituto di Ricerche Farmacologiche ''Mario Negri,'' 20157 Milano, Italy
(Received 22 September 1997; revised manuscript received 8 January 1998)

The kinetics of a cancer-cell population under the effects of an antitumoral drug is a topic of particular interest. Its theoretical understanding, along with the improvement of experimental investigation techniques, can indeed play an important role in antitumoral therapies development. Starting from the analysis of flow-cytometric data, with the aid of computer simulation we are able to give a detailed, quantitative description of the main kinetic parameters describing drug action on cancer cells. In this paper we describe the main features of our investigation method, showing an application to Igrov-1 ovarian carcinoma cells treated with cisplatin. Intermitotic time of phases, cell-cycle delay, and block effects with consequent repair or cell mortality, in a wide range of drug doses and recovery times, are discussed and interesting information about cisplatin action is found. [S1063-651X(98)11504-0]

PACS number(s): 87.10.+e

I. INTRODUCTION

One of the main features of cancer-cell populations is the lack of growth control. Normal cells proliferate either during embryogenesis and development of the organism or, more generally, whenever required by the organism itself. Most cells spend almost all their life in a quiescent state. But when a cell population becomes cancerous, this state of controlled reproduction is abandoned and the mitotic cycle becomes continuous. Of course the primary aim of antitumoral drug treatment is to kill or at least stop the proliferation of cancer cells. Thus the birth and development of tumors and the effects of clinical therapy can all be considered as changes in cell cycling. Hence the study of cancer-cell kinetics under the influence of drugs becomes a very interesting experimental and theoretical tool. A popular experimental technique utilized for studying cell-cycle kinetics is flow cytometry (FC) (an exhaustive description of this technique can be found in Ref. [1]), whose potential in providing important experimental data has still not been fully exploited. Especially since the introduction of recent phase-specific staining using monoclonal antibodies, the information conveyed by flow-cytometric measures is remarkable. Unfortunately, however, it is not always easy to interpret these data in terms of kinetic parameters, and sometimes it becomes ambiguous, as pointed out below. Without theoretical and computational support, quantitative results are hard to extract from flow-cytometric data. In order to avoid these interpretation problems, we developed a simulation program based on a realistic modelization of cell kinetics, which gives all the flow-cytometric observables as output. Once the experimental data are fitted by the simulation, a quantitative and detailed description of the kinetic scenario becomes possible, through estimates of a set of kinetic parameters governing cancer growth after drug treatment. Interpretation of the results in terms of the underlying molecular biology is beyond our intentions, and we shall limit our observation to cell population kinetics. We shall therefore omit details of the description of cell culture preparation, cytochemical techniques, or any discussion of the chemistry of the drug and its molecular mechanism of action against cancer cells (cisplatin cross-linking action on the DNA molecule is modeled in Ref. [2]). This paper concentrates on the interaction between ovarian cancer cells and cisplatin, one of the most important drugs in the therapy of this disease. Ovarian carcinoma is the sixth most frequent form of cancer worldwide (for a guideline on ovarian cancer, see Ref. [3]). Most patients respond to platinum-based first-line therapy, but untreatable relapse follows in most cases, leading to only 30% survival five years from diagnosis. From a pure kinetic point of view, cisplatin tends to block cancer cells in the last intermitotic phase, G_2 [4]. Effects on other phases (S and G_1) have been occasionally described [5]. However, no detailed, quantitative information is found in the literature, and cisplatin is still generally considered a G_2-blocking drug. In this work we will show that cisplatin action is much more complex, and present a quantitative description of its action in vitro on ovarian carcinoma Igrov-1 cells.

*Present address: Department of Biology, New York University, 1009 Main Building, New York, NY.

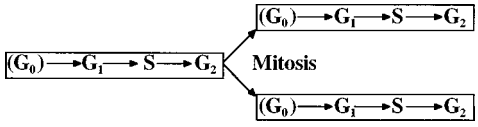

FIG. 1. A schematic cell-cycle representation

II. THEORY

A. Cell cycle

Mitotic cellular reproduction has been known to exist since the end of the last century. Between 1951 and 1953, Howard and Pelc [6,7] discovered that DNA synthesis marks just a central part of the cell's life. This observation suggested dividing the cell cycle into three *phases* of growth, plus the real mitotic event. Cells enter the cell cycle (see Fig. 1) in a first growth phase, called G_1. This is the period of life from the cell's birth till the beginning of DNA synthesis. In the S phase, cells duplicate their DNA. Then another gap is required before mitosis occurs: the G_2 phase. The last step is cell division, mitosis. In addition, cells may enter a quiescent state within G_1, called G_0. Many cells spend most of their life in G_0, without cycling. The study of the molecular events characterizing G_1, S, and G_2 phases is now a vigorous sector in cell biology. From the point of view of the numerical growth of a population of cancer cells, experimental evidence indicates periods of exponential growth, during which a steady state is reached, where the fraction of cells in every intermitotic phase is constant. This is called asynchronous growth. Using an elementary theory of asynchronous growth, it is possible to demonstrate [8] that the fraction of cells with age α from its birth, at the laboratory time t, is given by (see Fig. 2)

$$\frac{n(\alpha,t)}{N(t)} \propto e^{-c\alpha}. \tag{1}$$

In Eq. (1), c is the exponential growth constant of the population, $n(\alpha,t)$ the number of cells with age α at the observation time t, and $N(t)$ the overall cell number at the same time. Integrating this distribution over the phases times T_{G_1}, T_S, and T_{G_2}, the following relationships are obtained between the kinetic parameters (T_{G_1}, T_S, and T_{G_2} and their sum, the cell cycle time T_C) and the percentages of cells in the various phases ($\%G_1$, $\%S$, $\%G_2$):

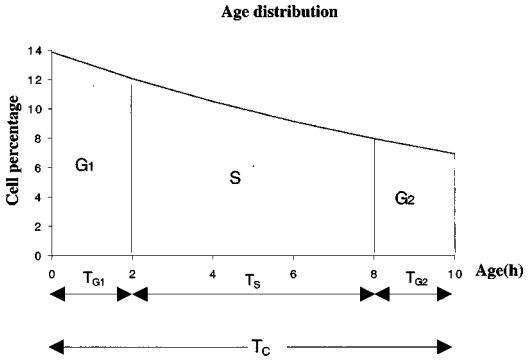

FIG. 2. Time-independent age distribution in asynchronous growth ($T_C=10$ h, $T_{G_1}=2$h, $T_S=6$ h in this example).

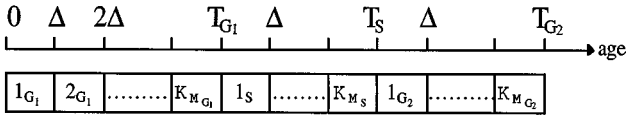

FIG. 3. Cell-cycle step division in the absence of intercell variability.

$$\frac{T_{G_2}}{T_C}=\frac{1}{\ln 2}\ln\left[1+\frac{\%G_2}{100}\right],$$

$$\frac{T_S}{T_C}=\frac{1}{\ln 2}\ln\left[1+\frac{\%G_2+\%S}{100}\right]-\frac{T_{G_2}}{T_C}, \tag{2}$$

$$\frac{T_{G_1}}{T_C}=1-\frac{T_S}{T_C}-\frac{T_{G_2}}{T_C}.$$

Equations (2) are valid if there is no intercell variability, i.e., if every cell is considered to spend exactly a time T_{G_1} in the G_1 phase, a time T_S in the S phase, and a time T_{G_2} in the G_2 phase. In Sec. III we will correct this assumption. Nevertheless it had been demonstrated [9] that Steel formulas are a good approximation for asynchronous growth, interpretating T_{G_1}, T_S, and T_{G_2} as mean phase durations.

Drug administration forces cells to leave asynchronous growth, their kinetics becoming much harder to describe. The main effects are (a) cell death; (b) cell-cycle phase delays; and (c) blocks: at the end of a particular phase, a cell only enters the next one if it passes an internal molecular check [10–12]. Drug-damaged cells can stop their cycle at the checkpoints.

Effects (a), (b), and (c) can be time dependent, giving rise to even more complex kinetics. Our model takes account of all these phenomena, simulating the consequences on real FC experimental data.

B. Cell-cycle simulation

Our computer program simulates cell cycling at different levels of complexity. At the lower level, we assume that all the cells of the population under investigation cycle in the same way, i.e., with no intercell differences in phase duration. It may be useful to divide the cell-cycle duration $T_C=T_{G_1}+T_S+T_{G_2}$ into a convenient number N of steps, each of a length Δ such that $T_C=N\Delta$ (see Fig. 3). Let $G_1(k,t)$ be the number of cells in the kth step of G_1 [grouping cells with age between $(k-1)\Delta$ and $k\Delta$] at a certain time t, similar definitions holding for $S(k,t)$ and $G_2(k,t)$. The time course of $G_1(k,t)$, $S(k,t)$, and $G_2(k,t)$ from t to $t+\Delta$ is immediately obtained considering the following set of equations:

$$G_2(k+1,t)=G_2(k,t-\Delta),$$

$$1_{G_2}<k\leqslant k_{MG_2} \quad \left(k_{MG_2}=\frac{T_{G_2}}{\Delta}\right),$$

$$G_2(1_{G_2},t)=S(k_{M_S},t-\Delta),$$

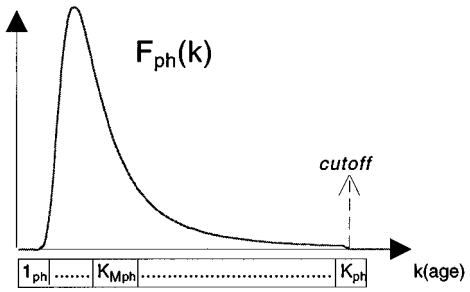

FIG. 4. When intercell variability is considered, T_{ph} becomes just the mean value of the time each cell spends in a phase before leaving it. Each phase is now characterized by a function $F_{\mathrm{ph}}(\alpha)$, giving the probability of completing a phase in a time α. After a few standard deviations from the mean, $F_{\mathrm{ph}}(\alpha)$ can be cut off to zero. We used K_{ph} to indicate the last value of k for which F_{ph} is not zero.

$$
\begin{aligned}
&S(k+1,t)=S(k,t-\Delta), \quad 1_S<k\leqslant k_{M_S} \quad \left(k_{M_S}=\frac{T_S}{\Delta}\right),\\
&S(1_S,t)=G_1(k_{M_{G1}},t-\Delta),\\
&G_1(k+1,t)=G_1(k,t-\Delta), \quad 1_{G_1}<k\leqslant k_S \quad \left(k_{MG_1}=\frac{T_{G_1}}{\Delta}\right),\\
&G_1(1_{G_1},t)=2G_2(k_{M_{G2}},t-\Delta).
\end{aligned}
\tag{3}
$$

At the second level of complexity, intercell variability of the phase duration is considered, meaning that not all the cells spend the same time T_{ph} in each phase (from here on ph will indicate G_1, S, or G_2). There will be a probability distribution $F_{\mathrm{ph}}(k)$, giving the likelihood of a cell of phase age k leaving the phase. Experimentally it has been observed [13] that a good approximation for $F_{\mathrm{ph}}(k)$ is a reciprocal-normal distribution, though what follows is independent of the choice, the only assumption being that $F_{\mathrm{ph}}(k)$ is a two-parameter distribution, fully specified if the first two moments are known. It is convenient to consider three different cell-cycle step divisions, one for each phase, and three probability distributions of phase transit times F_{ph}. The input set of kinetic parameters is now $\{T_{G_1},T_S,T_{G_2},CV_{G1},CV_S,CV_{G2}\}$, where T_{G_1}, T_S, and T_{G_2} are mean times of phases, and CV_{G1}, CV_S, and CV_{G2} are the coefficients of variation of the probability distributions (given by the ratio of standard deviation to the mean). Note that $F_{\mathrm{ph}}(k)$ does not need to be zero $k>k_{M_{\mathrm{ph}}}$: that is exactly what intercell variability means (see Fig. 4). In practice, the reciprocal-normal distributions $F_{\mathrm{ph}}(k)$ were cut off for $k=K_{\mathrm{ph}}$ exceeding six standard deviations from the mean phase duration and then consequently normalized.

Once the factor

$$
D_{\mathrm{ph}}(k)=\frac{F_{\mathrm{ph}}(k)}{\left[1-\sum_{j=1}^{k-1}F_{\mathrm{ph}}(j)\right]} \tag{4}
$$

is introduced, it is not hard to verify (for more details, see Ref. [14]) that the system equations are

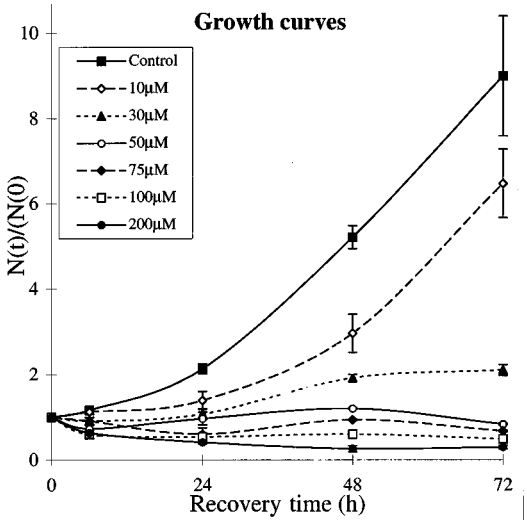

FIG. 5. Growth curves measured with a Coulter counter. Our population was divided into different tissue-culture flasks; error bars arise from three different flask counts. In this graph, the cell number is normalized over the initial number of untreated cells (i.e., over the control 0-h number of cells).

$$
\begin{aligned}
&G_2(k+1,t)=G_2(k,t-\Delta)[1-D_{G_2}(k)],\\
&G_2(1_{G_2},t)=\sum_{k=1}^{K_S}S(k,t-\Delta)D_S(k),\\
&S(k+1,t)=S(k,t-\Delta)[1-D_S(k)],\\
&S(1_S,t)=\sum_{k=1}^{K_{G_1}}G_1(k,t-\Delta)D_{G_1}(k),\\
&G_1(k+1,t)=G_1(k,t-\Delta)[1-D_{G_1}(k)],\\
&G_1(1_{G_1},t)=2\sum_{k=1}^{K_{G_2}}G_2(k,t-\Delta)D_{G_2}(k).
\end{aligned}
\tag{5}
$$

In the third level of complexity, the mitotic event is considered in greater detail. We introduced p_{mit}, the mean number ($\leqslant 2$) of living newborn cells originating from a mitotic event, and the precycle phase G_0. We simulated G_0 as a single-compartment phase, so no k index is needed, assuming first-order exit kinetics. Moreover, newborn cells (i.e., p_{mit} times the number of cells exiting G_2) have a probability bp_{G0} of bypassing G_0 (thus $1-bp_{G_0}$ represents the probability of moving into G_0). Once a cell falls into G_0, p_{G0G1} is the chance it has of leaving G_0 and entering G_1 with every time step. The equation for G_0 adds to Eqs. (5), where the $G_1(1,t)$ equation also changes:

$$
\begin{aligned}
G_1(1_{G_1},t)&=G_0(t-\Delta)p_{G0G1}\\
&\quad+bp_{G0}p_{mit}\sum_{k=1}^{K_{G_2}}G_2(k,t-\Delta)D_{G_2}(k),\\
G_0(t)&=G_0(t-\Delta)(1-p_{G0G1})\\
&\quad+(1-bp_{G0})p_{mit}\sum_{k=1}^{K_{G_2}}G_2(k,t-\Delta)D_{G_2}(k).
\end{aligned}
\tag{6}
$$

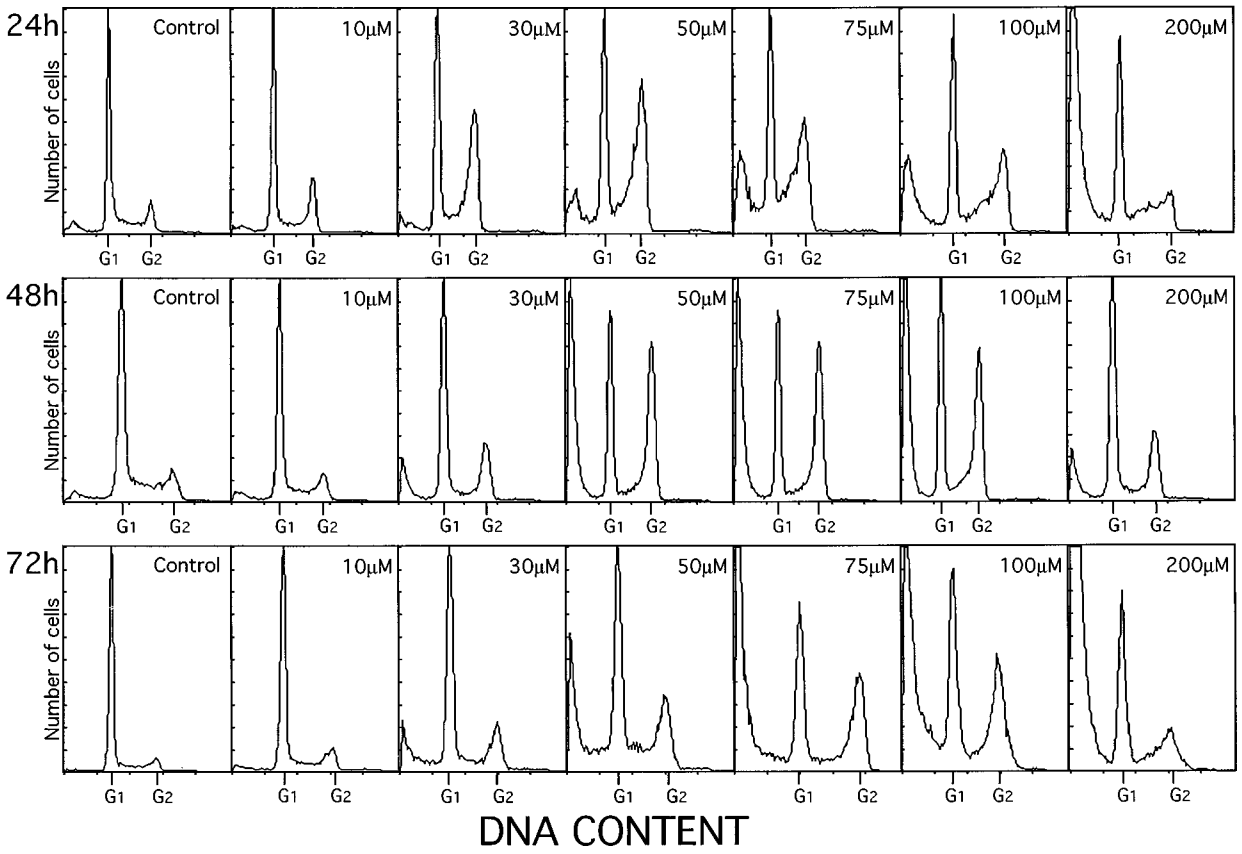

FIG. 6. DNA histograms measured 24, 48, and 72 h after cisplatin treatment at the indicated doses. Cells deriving from three replicated flasks, i.e., independently treated with the same dose, were pooled, and 10 000 cells from the pool were analyzed and represented in each frequency histogram. DNA content corresponding to G_1 and G_2 cells is indicated. G_2 peak position is double G_1, confirming the stoichiometric DNA-PI binding. An accumulation of cells in the G_2 peak is particulary evident in the 50- and 75-μM histograms.

The highest complexity level takes into account the kinetic effect of a drug. Cells can be blocked, particularly at the checkpoints at the end of G_1 and G_2, or they can be generally slowed down in their cycle. Entering a cell-cycle phase, they may stop cycling, becoming definitively quiescent. They can also be killed by the drug at a distinct rate in every phase. Blocks are simulated using the parameters $p_{\mathrm{ph}}B^{\mathrm{in}}$, representing the fraction of cells entering a specific compartment of blocked cells, out of the cells which, following Eqs. (5) and (6), should live their phases at a certain time step. Blocked cells may either repair the damage caused by the drug and recycle, or die in the block. The probabilities of these events are $p_{\mathrm{ph}}B^{\mathrm{out}}$ and $p_{\mathrm{ph}}B^{\mathrm{die}}$. Freezing acts differently, inhibiting the age maturation of a fraction $p_{\mathrm{ph}}F$ of nonblocked cells which populates a certain phase ph at the laboratory time t. Obviously, until they are frozen, cells are not able to change their age compartment. Freezing can also drive cells to death: in our simulation $p_{\mathrm{ph}}Fp_{\mathrm{ph}}F^{\mathrm{die}}$ frozen cells are eliminated every time step. The overall effect of freezing is a delay in the mean transit time in a given phase. Cells entering a given phase may otherwise become definitively quiescent with a probability $p_{\mathrm{ph}}Q$. Quiescent cells accumulate in a specific compartment Q, in which death occurs with a probability $p_{\mathrm{ph}}Q^{\mathrm{die}}$ every time step. Last, we considered proliferating cell loss, as a possible direct effect of the drug regardless of cell cycle perturbations. This was simulated by introducing a nonzero probability $p_{\mathrm{ph}}^{\mathrm{die}}$ of leaving the cell population. Introducing all these parameters, we did not explicitly introduce their time dependence, so as to simplify our formalism, but we are able to consider it. This is crucial, because it is biologically clear that blocks, delays, and death are time dependent. Taking all real drug effects into account, we are now ready to compare our simulations with experimental results. Final system equations should be easy for the reader to compute, though formally heavy, and are given in Appendix A.

One of the most interesting types of experimental FC information comes from the analysis of bromodeoxyuridine (BrdUrd)-labeled cells. Our program simulates this too, by dividing each phase-occupation number distribution $\mathrm{Ph}(k,t)$ into positive-BrdUrd and negative-BrdUrd distributions. In practice, at a given labeling time, every cell in the S phase becomes BrdUrd positive, filling $S^+(k,t)$. After that time, the evolution of positive and negative cells is followed, considering that a positive cell which doubles gives two positive cells, and that the presence of BrdUrd does not change the already discussed evolution equations. Thus, the program computes two parallel cycles, one describing $G_0^-(k,t)$, $G_1^-(k,t)$, $S^-(k,t)$, and $G_2^-(k,t)$, and the other $G_0^+(k,t)$, $G_1^+(k,t)S^+(k,t)$, and $G_2^+(k,t)$. Obviously $\mathrm{Ph}(k,t) = \mathrm{Ph}^-(k,t) + \mathrm{Ph}^+(k,t)$.

III. EXPERIMENTAL METHODS

Igrov cancer cells *in vitro* in their exponential phase of growth were treated for one hour with cisplatin at different

doses, from 10 to 200 μM. Cell kinetics after treatment was measured using standard flow-cytometric techniques and by counting the cells with a Coulter counter. The flow-cytometer (Becton Dickinson FACSort) and Coulter counter (Coulter Electronics ZM) are commercial machines. When required, BrdUrd (the role of this nucleotide is explained here, but for a review concerning its use in FC, see Ref. [15]) was added at the end of drug treatment. Then the drug and BrdUrd were washed away, and cells were left in a free-drug culture medium for the recovery times indicated. At the end of recovery, cells were detached, counted (Fig. 5 shows its growth curves), and fixed in cold 70% ethanol. Fixed cells underwent cytochemical and immunocytochemical treatments with the appropriate probes and were analyzed by FC.

One-parametric DNA analysis using propidium (PI) iodide staining

Fixed cells were stained with 2 μg/ml of PI in phosphate buffer saline. PI is a fluorescent DNA probe which intercalates between DNA base pairs in a stoichiometric way (for a review concerning PI staining, see Ref. [16]). These cells are then analyzed with the FC, passing one at a time through an argon laser beam ($\lambda = 488$ nm), producing a PI fluorescent signal proportional to their DNA content. Fluorescence pulses are detected by a photomultiplier tube (PMT), amplified by an electronic chain and the measures of their integral intensities (again proportional to the DNA content of the single cells [17]) are memorized by the dedicated computer. Signals from at least 10 000 cells were collected, giving frequency histograms for the cellular DNA content in the cell population under study (see Fig. 6). DNA histograms were analyzed using a previously described software [18], obtaining $\%G_1$, $\%S$, and $\%G_2$.

Two-parametric FC analysis of cellular DNA content and BrdUrd incorporation

The status of DNA synthesizing cells at the end of treatment was probed by pulse treatment with BrdUrd. *S*-phase cells incorporate BrdUrd instead of thymidine during DNA synthesis. After fixing, BrdUrd was detected by a specific antibody (FITC-anti-BrdUrd) conjugated to a fluorochrome, as previously described [19]. PI and FITC-anti-BrdUrd fluorescence pulses were measured on the same cell at the same time by two PMT's, placed at the end of two distinct optical paths selecting the not-overlapping wavelength ranges characteristic of PI (600–660 nm) and FITC (515–545 nm) fluorescence emissions. In this way, biparametric histograms such as those presented as dot plots in Fig. 7 are obtained. For a 0-h recovery time, cells labeled by FITC-anti-BrdUrd (BrdUrd-*positive*) are exactly *S*-phase cells, while *negative* cells are part G_1 and part G_2 phases, distinguishable by their DNA content. Later on, BrdUrd-positive cells maintain their label, allowing their recognition while crossing the successive G_2, transmitting the label to their descendants entering G_1, and so on. Thus, at any time, BrdUrd-positive cells are cells that were in the *S* phase at the time of treatment, or their descendents. In our experimental plan, this long and costly analysis was done at 0- and 6-h recovery times. Additional BrdUrd measures at particular recovery times are still possible, to resolve simulation scenarios equally fitting the other data.

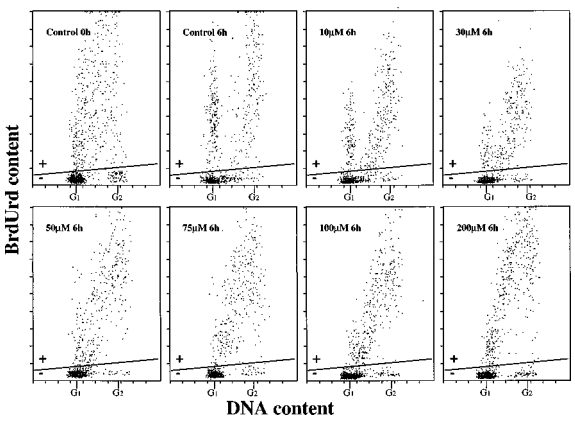

FIG. 7. Biparametric PI-fluorescence (DNA content) and FITC-fluorescence (BrdUrd contnent) plots, 6 h after treatment. The diagonal line separates BrdUrd positive cells (in the *S* phase at the time of labeling, i.e., at 0 h) from BrdUrd-negative ones (in G_1^- and G_2^- phases at the labeling time). Negative cells do not give a zero signal because of a small overlap between PI and FITC emission spectra. Cells derving from three replicated flasks were pooled, and 10 000 cells from the pool were analyzed. BrdUrd-positive cells with G_1 DNA content were born (in the time interval 0–6 h) from mitosis of cells in *S* phase at the drug treatment time. Few of them are detected in samples treated at doses higher than 50 μM. Not yet divided BrdUrd-positive cells are found at the end of the *S*-phase (the DNA content is close to the G_2 peak) and in G_2 (always at 6 h) in controls. Many of them are still at the beginning and in the middle of the *S* phase in treated samples at doses higher than 50 μM.

IV. RESULTS

A. Qualitative analysis of the measures

A certain amount of qualitative information can be obtained by visual inspection of the rough experimental data (Figs. 5, 6, and 7). Figure 5 is the easiest to interpret. When no drug is present (control data), the growth is, as expected, exponential (the curve

$$N(t) = N(0)e^{t(\ln 2/T_c)}$$

fits the data with $T_C = 19.95h$, $r^2 = 0.996$). Growth inhibition was already apparent after 10 μM, and became strong at the dose of 30 μM. For higher doses cell loss is clearly demonstrated by the decline in the growth curves. Figure 6 gives a more precise idea of drug effects. Low (lower than G_1) DNA content cells were observed at high doses. These signals were due to cellular debris containing small portions of

TABLE I. Cell-cycle percentages and phase durations: comparison between experimental data (untreated control samples), simulated results and Steel estimates [Eq. (2)].

	$\%G_1$	$\%S$	$\%G_2$
Expt.	56	34.5	9.5
Sim.	56	34.5	9.5
	T_{G_1}	T_S	T_{G_2}
Steel [Eq. (2)]	9.5	7.9	2.6
Sim.	9.5	8	2.5

TABLE II. Experimental and simulated data at 24, 48, and 72 h. N is the total number of cells normalized on the initial number before drug treatment (0-h control). $\%G_1$, $\%S$ and $\%G_2$ are obtained from the DNA histograms shown in Fig. 6. The drug doses unit is μM.

Dose	Time	$\%G_1$(expt.)	$\%G_1$(sim.)	$\%S$(expt.)	$\%S$(sim.)	$\%G_2$(expt.)	$\%G_2$(sim.)	N(expt.)	N(sim.)
10	24	52	51	29	30	19	19	1.39±0.21	1.58
10	48	60	59	30	31	9	10	2.96±0.45	3.14
10	72	57	58	35	33	8	9	6.48±0.81	6.27
30	24	35	35	30	30	36	35	1.07±0.12	0.99
30	48	51	50	31	31	19	19	1.92±0.08	1.86
30	72	57	55	28	29	15	16	2.10±0.13	2.21
50	24	31	31	31	33	38	36	0.96±0.11	0.89
50	48	43	41	19	22	38	37	1.20±0.02	1.23
50	72	46	48	36	33	18	19	0.84±0.07	0.92
75	24	35	34	41	39	24	27	0.60±0.15	0.72
75	48	35	37	24	23	41	40	0.94±0.02	0.93
75	72	39	39	32	32	29	30	0.68±0.02	0.67
100	24	35	35	39	38	26	26	0.54±0.04	0.57
100	48	40	38	28	29	32	32	0.60±0.02	0.58
100	72	32	35	36	33	32	33	0.49±0.04	0.52
200	24	45	45	41	42	14	13	0.41±0.04	0.40
200	48	45	46	40	39	15	16	0.26±0.07	0.26
200	72	42	44	38	38	20	19	0.30±0.05	0.25

DNA, originating from cells destroyed by the drug treatment, and are indicative of cell death. G_1, S, and G_2 percentages, calculated from DNA histograms, are reported in Tables I (untreated cells) and II (treated cells). From a qualitative point of view, 10 μM of cisplatin induced only a slight, temporary (at 24 h) increase in the G_2 percentage. At 30 μM, at 24 h, the G_2 increase was more evident. This means that part of the cells in this phase were blocked. The population in G_2 declined at subsequent times. Increasing the dose to 50 μM, the G_2 block was more stable in time. Very similar situations, always from a qualitative point of view, were found at 75 and 100 μM, while for the highest dose (200 μM) a very large amount of cellular debris was observed. Figure 7 shows a biparametric PI-FITC-anti-BrdUrd plot, with the corresponding numerical data shown in Table III. At $t=6$ h, part of the BrdUrd-positive cells, in the S phase at $t=0$ h, had time to divide, reaching G_1. T_S occuring around 8 h, another part of the BrdUrd-positive cells was still crossing the late S phase and G_2. Note that the 10- and 30-μM plots are similar, suggesting that the divergence of the effects, observed in DNA histograms at $t=24$ h, occurs later, possibly on daughters of treated cells. At higher doses (50 and 75 μM), positive cells clearly reduce the cycling speed, as demonstrated by the fact that the cloud of BrdUrd-positive cells is only slightly shifted to the right in 6 h. This effect is even more evident for the two highest doses, whose biparametric graph is very similar to the 0-h one, indicating an almost total cycle freeze. This qualitative assessment of results cannot proceed further, even it presents some ambiguity, because the percentage of cells blocked, say, in G_2, is dependent on the delays, blocks and deaths, experienced by the cells in the other phases before reaching the G_2 checkpoint. Moreover, cell death can be argued from the decline of the growth curve, but its connection with cell-cycle events cannot be directly inferred by simple examination of the histograms.

B. Simulations

The task of the computer simulation is to consider all experimental data together, with a number of drug doses and recovery times, to give a complete coherent kinetic scenario,

TABLE III. Eperimental and simulated percentages and cell number (N) at 6 h. Cell percentages are calculated from the biparametric PI-FITC-anti-BrdUrd graphs shown in Fig. 7. $\%\text{tot}^+$ is the percentage of BrdUrd-positive cells, while $\%1\text{C}^+$ is the percentage of undivided BrdUrd-positive cells, still in S and G_2 phases. The drug dose unit is μM.

Dose	Time	tot^+(expt.)	tot^+(sim.)	1C^+(expt.)	1C^+(sim.)	G_1^-(expt.)	G_1^-(sim.)	N(expt.)	N(sim.)
10	6	36	37	24	24	43	43	1.13±0.06	1.10
30	6	32	34	26	27	55	53	0.91±0.08	0.87
50	6	36	36	32	32	56	56	0.73±0.06	0.81
75	6	35	35	31	31	60	59	0.91±0.08	0.80
100	6	28	29	25	25	65	64	0.60±0.09	0.64
200	6	32	30	31	29	61	62	0.64±0.06	0.58

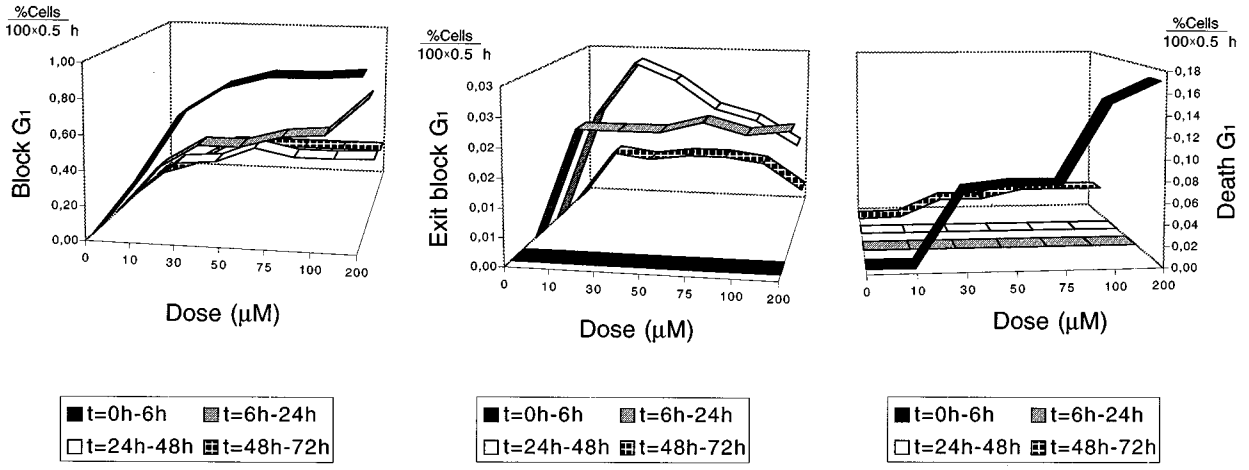

FIG. 8. Parameters describing the effect of the drug in the G_1 phase, in the scenario fitting the whole set of FC and cell number data. *Block* G_1 represents $p_{G_1}B^{\text{in}}$ (the fraction of cells exiting the block in 0.5 h out of cells leaving G_1. *Exit block* G_1 represents $p_{G_1}B^{\text{out}}$ (the fraction of cells exiting the block in 0.5 h out of G_1 blocked cells). *Death* G_1 represents $p_{G_1}B^{\text{die}}$ (the fraction of cells which die in 0.5 h out of G_1 blocked cells).

with a quantitative estimate of block duration and strength in each phase, filtered for the consequences of other phase alterations. Once the input baseline set of kinetic parameters $\{T_{G_1}, T_S, T_{G_2}, CV_{G_1}, CV_S, CV_{G_2}\}$ was determined, fitting the data of untreated cells (see Table I for a comparison between Steel results and simulated data), we started to simulate the data on cisplatin-treated cells, with a trial-and-error procedure, always based on a biological knowledge of the phenomena. To reduce the redundancy of descriptive parameters, drug effects on G_1 and G_2 were described only by block parameters, and those on the *S* phase by freezing parameters. This choice is biologically sustainable, since G_1 and G_2 molecular checkpoints are known to be active in intercepting damaged cells, blocking them until the damage is repaired or cell death occurs, while there is not a definite checkpoint in the *S* phase. Another biological assumption is that cell death is an end point that follows blocking or, at least, slowing down of biological functions and cell-cycle progression, unless very high drug exposure causes immediate disruption of the cell. Moreover, biological coherence imposes a trend of some drug effects over time and dose, which led us to eliminate, for example, the fittings obtained with reduction of deaths with increasing dose as biologically unfair scenarios. We assumed for all parameters a simplified time dependence, considering them constant within the observation intervals (0–6, 6–24, 24–48, and 48–72 h). Thus parameter values should be interpreted as mean values in the given interval. We used a 0.5-h time step, which means a very high temporal resolution compared to typical intervals of data collection in FC experiments. Because simulation parameters are reported in units of cell%/(100 time steps), a cell death of, for example, 0.1 among G_2-phase blocked cells means that 10% of the total number of G_2-phase blocked cells at that time die every 30 min. Because the experimental

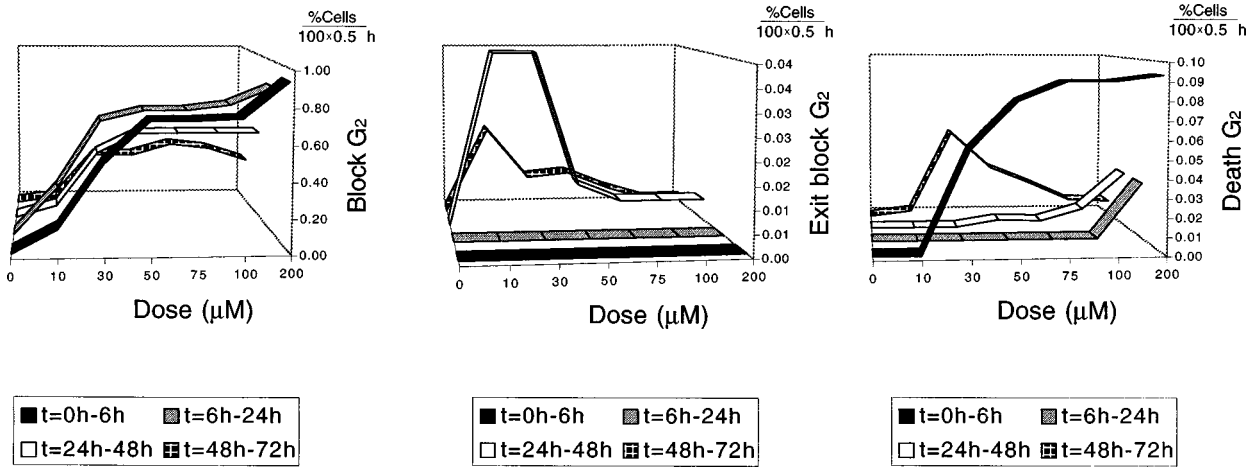

FIG. 9. Parameters describing the effect of the drug in the G_2 phase, in a scenario fitting the whole set of FC data. *Block* G_2 represents $p_{G_2}B^{\text{in}}$ (the fraction of cells exiting the block in 0.5 h out of cells leaving G_2). *Exit block* G_2 represents $p_{G_2}B^{\text{out}}$ (the fraction of cells exiting the block in 0.5 h out of G_2 blocked cells). *Death* G_2 represents $p_{G_2}B^{\text{die}}$ (the fraction of cells which die in 0.5 h out of G_2 blocked cells).

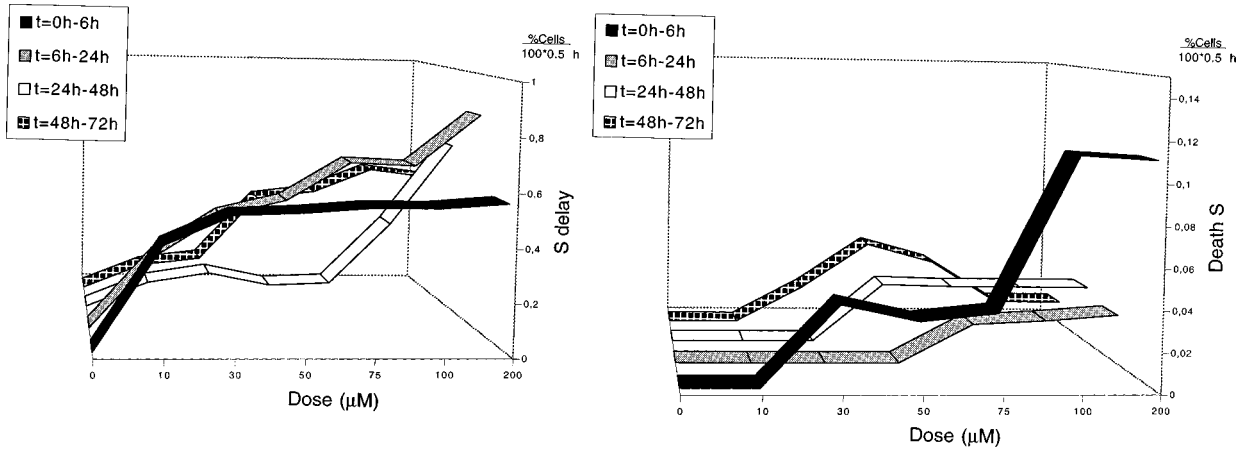

FIG. 10. Parameters describing the effect of the drug in the *S* phase, in the scenario fitting the whole set of FC data. *S Delay* represents $p_S F$ (the fraction of cells *frozen* in 0.5 h out of *S*-phase cells). *Death S* represents $p_S F^{\text{die}}$ (the fraction of cells which die in 0.5 h out of *S* frozen cells).

precision of FC percentages is about 3%, and cell counts 10%, the fitting was considered satisfactory when the experimental data were reproduced with the same precision. Our initial plan was to find, by trial-and-error procedure, more than one biologically appropriate scenario, and challenge the alternatives by specific additional measures, as should have been suggested by the simulation itself. However, no reasonable alternative to the scenario outlined below was found. All attempts to fit the data limiting the drug effect to one or two phases were unsuccessful (in Appendix B we shall discuss this point in more detail, giving a practical example of the fitting procedure). Thus the first feature of the resulting scenario is that perturbations have been introduced in every phase. Figures 8, 9, and 10 show the dose and time dependence of the block, repair, and death parameters (or delay parameter for the *S* phase).

G_1 phase (see Fig. 8)

Cisplatin blocks G_1 cells in all recovery times we analyzed. The block strength is maximum during the first period (say 6 h) after treatment. Subsequently the effect becomes weaker but it is always noticeable. Looking at the dose dependence, the block already manifests itself strongly at 30 μM. At higher doses, no significant changes in block strength are detected. Block repair is prompt, for already in the period 6–24 h, and exit was allowed for. In our scenario, repair was easier at low doses. A G_1 block induces an immediate, strong loss effect, increasing with dose. After the initial recovery times, cell death seems negligible in a wide range of observation times (6–48 h). Only after 48 h does cell loss become appreciable again.

G_2 phase (see Fig. 9)

The G_2 block is continuous in time as well. It does not appear to weaken significantly during the whole period we analyzed. Only between 48 and 72 h do the cisplatin effect on G_2 cells seem weaker. Raising the drug dose from 10 to 50 μM, the block rapidly becomes stronger. After 50 μM, on the other hand, no significant increases in block strength are seen. Repair is possible only for low and intermediate doses, and takes more time than for the G_1 block. Cell-loss analysis for the G_1 block seems to be valid for G_2 too: indeed, there is a strong dose-related loss in the first hours after drug treatment. A small difference may be found for longer recovery times: low and intermediate doses seem more effective in killing cells between 48 and 72 h, while no loss is seen between 6 and 48 h. The highest doses (100 and 200 μM), have a continuous loss effect; 200 μM causes cell death from 0 to 72 h, while 100 μM do not kill cells only between 6 and 24 h.

S phase (see Fig. 10)

Cisplatin slows the *S*-cell cycle. The *S*-phase delay is shown in Fig. 10 (left panel), as measured by the parameter $p_S F$, as explained in Sec. II. The value of $p_S F$ in the first 6 h after treatment, for doses higher than 30 μM, is close to 0.6, which corresponds to a 100% increase in the time of the *S* phase. Only 200 μM causes a strong *S*-phase delay, continuous over time. At intermediate doses, there is a *biphasic* behavior: the *S* delay is noticeable at first (0–6 h), increasing slightly until 24 h but decreasing from 24 and 48 h to reach its original strength again at the final observation

TABLE IV. Percentages of G_1 (upper table) and G_2 (lower) blocked cells in the scenario fitting the whole set of FC and cell number data.

% of G_1 blocked cells						
Time (h)	10 μM	30 μM	50 μM	75 μM	100 μM	200 μM
0	0	0	0	0	0	0
6	9.2	17.5	22.2	24.6	21.6	22.0
24	14.3	20.7	21.6	27.1	30.1	42.3
48	12.6	10.8	13.9	15.4	18.2	28.9
72	8.5	13.7	15.4	11.1	10.1	14.0
% of G_2 blocked cells						
Time (h)	10 μM	30 μM	50 μM	75 μM	100 μM	200 μM
0	0	0	0	0	0	0
6	2.0	5.9	7.9	7.4	8.7	11.9
24	12.6	28.1	29.9	25.3	24.5	12.2
48	2.5	10.6	30.0	33.8	28.3	11.6
72	1.4	7.6	12.9	24.4	28.5	14.8

time. For the lowest doses (10 and 30 μM) the S delay decreases with time. S-cell loss seems important only at the highest doses, and during the first hours after treatment. Nevertheless for all doses over 10 μM cisplatin can cause S-cell death, especially just after treatment and after a long recovery time.

V. DISCUSSION AND CONCLUSIONS

We developed a simulation model of the cell cycle, with the intention of creating a useful tool for researchers. In this research field, involving scientists from different disciplines, one of the main problems is the distance between theoretical and experimental approaches. Our simulation program runs on an ordinary Pentium PC, is easy to handle, and gives results directly comparable with experimental ones. Its mathematical machinery is perhaps less refined than other purely theoretical models proposed in the cancer-cell kinetics field (for a review, see Ref. [20]), but it is fully based on parameters with a clear biological meaning, and allows a link with experimental data. In this paper we described the kinetic effects of cisplatin on Igrov-1 cells. Our simulation program enabled us to find a scenario satisfactorily fitting all data, with a smooth dose dependence. This gave us a detailed description of block, delay, repair, and death effects. We do not claim that the set of simulation parameters we found is the only one to fit all the data. However, we found no alternative biologically coherent picture of the events, fully compatible with our set of more than 120 data at different times and doses. The simulation results indicated that at a given time, block strength increases with the dose, while the time dependence is more complex. Cisplatin acts immediately on cells in the G_1 phase, at all the doses we analyzed, while cells treated with lower doses in the last cell cycle phases experience a milder G_2 block that cells subsequently reaching the G_2 checkpoint. As we pointed out, cisplatin is commonly known as an antitumoral drug that blocks cells in G_2. Table IV reports simulated percentages of G_1 and G_2 blocked cells. Our data confirm the G_2 block as a very important kinetic effect caused by cisplatin on Igrov-1 cells but, at the same time, show the fundamental role of the G_1 block. After a recovery time of 24 h, G_1 blocked cells, for example, are between 14% (10 μM) and 43% (200 μM) of the total population. Note that at 24 h for a dose of 200 μM, histograms give a total G_1 occupation of 45%; this means that almost every cell in G_1 is blocked at this time. This effect was completely hidden by histogram plots alone: going back to Fig. 5, and comparing control ($\%G1=56\%$) and 200 μM ($\%G1=45\%$), it would have been impossible to infer the existence of a G_1 block. Only with a simulation able to consider G_1, S, and G_2 occupation percentages together with the growth curve was it possible to detect the G_1 block and estimate its strength. We were able to describe the fate of blocked cells, from the time course of repair and death probabilities. They describe the block in more detail, giving information not included in the block strength. $p_{\mathrm{ph}}B^{\mathrm{out}}$ and $p_{\mathrm{ph}}B^{\mathrm{die}}$ act on blocked cells, so that to evaluate the importance — that is the number of cells exiting — in repair or death at a certain time t, one must multiply them by percentage of the blocked cells at that time (reported in Table IV). No repair was observed in the first 6 h (Figs. 8 and 9, second panels), meaning that it takes longer to complete the sequence *checkpoint block* plus *DNA repair*. During the second observation period (6–24 h), G_1 and G_2 blocks show different behaviors, the latter being closed, while some G_1 cells exit from their block. This suggests different behaviors of the two blocks, the G_2 block needing a longer repair time. Between 24 and 48 h and during the last observation period (48–72 h), both G_1 and G_2 blocked cells repair. Again, the G_2 block looks stronger because cell repair is negligible at medium and high doses. As regards the time course of death, the death rate was high in the first hours with all doses greater than 10 μM, regardless of the phase. Thus there is initial cisplatin toxicity, leading to cell death in a short time. At the highest dose (200 μM), up to 50% of the initial population dies in the first 6 h and most surviving cells remain blocked thereafter. Between 6 and 48 h, the death rate is negligible for all doses except 200 μM. Cell death rises again only in the last 24 h of observation. This kind of time dependence can be interpreted as meaning that most sensitive cells die in a short time during and after treatment; subsequently, the drug induces blocks and freezing. Cells blocked in the central period of our observation, which are too damaged for repair, die at later times. In conclusion, on account of its continuous and prolonged action, the low number of repairing cells, and the time required for repair to start, the G_2 block can be considered the major effect of low and/or intermediate cisplatin doses on ovarian carcinoma cells. However the G_1 block and S delay, with peculiar kinetic characteristics, are also active, and make a substantial contribution to the drug's effect. We want to emphasize that our cell-kinetics analysis method can be applied without additional problems to any other cancerous population — antitumoral drug system. In this paper we presented our first application, but we are confident we will be soon able to collect and analyze much more data, so that quantitative comparisons between different drugs action on a particular cancerous population will be possible.

APPENDIX A: COMPLETE SET OF EQUATIONS DESCRIBING DRUG EFFECTS ON CANCER CELLS IN OUR MODEL

Here we want to report the full equations system utilized to reach the results described in this paper.

$$G_2(k+1,t)=G_2(k,t-\Delta)[1-D_{G_2}(k)](1-p_{G_2}F)(1-p_{G_2}^{\mathrm{die}})+G_2(k+1,t-\Delta)p_{G_2}F(1-p_{G_2}F^{\mathrm{die}}),$$

$$G_2(1,t)=\left[S(B,t-\Delta)p_SB^{\mathrm{out}}+(1-p_SB^{\mathrm{in}})\sum_{k=1}^{K_S}S(k,t-\Delta)D_S(k)(1-p_SF)(1-p_S^{\mathrm{die}})\right](1-p_{G_2}Q)(1-p_{G_2}^{\mathrm{die}})$$

$$+G_2(1,t-\Delta)p_{G_2}F(1-p_{G_2}F^{\mathrm{die}}),$$

$$G_2(B,t)=G_2(B,t-\Delta)(1-p_{G_2}B^{\mathrm{out}})(1-p_{G_2}B^{\mathrm{die}})+p_{G_2}B\sum_{k=1}^{K_{G_2}}G_2(k,t-\Delta)D_{G_2}(k)(1-p_{G_2}F)(1-p_{G_2}^{\mathrm{die}}),$$

$$G_2(Q,t)=\left\{\left[S(B,t-\Delta)p_SB^{\mathrm{out}}+(1-p_SB^{\mathrm{in}})\sum_{k=1}^{K_S}S(k,t-\Delta)D_S(k)(1-p_SF)(1-p_S^{\mathrm{die}})\right]p_{G_2}Q+G_2(Q,t-\Delta)\right\}(1-p_{G_2}Q^{\mathrm{die}}),$$

$$S(k+1,t)=S(k,t-\Delta)[1-D_S(k)](1-p_SF)(1-p_S^{\mathrm{die}})+S(k+1,t-\Delta)p_SF(1-p_SF^{\mathrm{die}}),$$

$$S(1,t)=\left[G_1(B,t-\Delta)p_{G_1}B^{\mathrm{out}}+(1-p_{G_1}B^{\mathrm{in}})\sum_{k=1}^{K_{G_1}}G_1(k,t-\Delta)D_{G_1}(k)(1-p_{G_1}F)(1-p_{G_1}^{\mathrm{die}})\right](1-p_SQ)(1-p_S^{\mathrm{die}})$$
$$+S(1,t-\Delta)p_SF(1-p_SF^{\mathrm{die}}),$$

$$S(B,t)=S(B,t-\Delta)(1-p_SB^{\mathrm{out}})(1-p_SB^{\mathrm{die}})+p_SB\sum_{k=1}^{K_S}S(k,t-\Delta)D_S(k)(1-p_SF)(1-p_S^{\mathrm{die}}),$$

$$S(Q,t)=\left\{\left[G_1(B,t-\Delta)p_{G_1}B^{\mathrm{out}}+(1-p_{G_1}B^{\mathrm{in}})\sum_{k=1}^{K_{G_1}}G_1(k,t-\Delta)D_{G_1}(k)(1-p_{G_1}^{\mathrm{die}})(1-p_{G_1}F)\right]p_{G_1}Q+S(Q,t-\Delta)\right\}$$
$$\times(1-p_SQ^{\mathrm{die}}),$$

$$G_1(k+1,t)=G_1(k,t-\Delta)[1-D_{G_1}(k)](1-p_{G_1}F)(1-p_{G_1}^{\mathrm{die}})+G_1(k+1,t-\Delta)p_{G_1}F(1-p_{G_1}F^{\mathrm{die}}),$$

$$G_1(1,t)=\left\{\left[G_2(B,t-\Delta)p_{G_2}B^{\mathrm{out}}+(1-p_{G_2}B^{\mathrm{in}})\sum_{k=1}^{K_{G_2}}G_2(k,t-\Delta)D_{G_2}(k)(1-p_{G_2}F)(1-p_{G_2}^{\mathrm{die}})\right]p_{\mathrm{mit}}bp_{G0}\right.$$
$$\left.+G_0(t-\Delta)p_{G0G1}(1-p_{G_0}^{\mathrm{die}})\right\}(1-p_{G_1}Q)(1-p_{G_1}^{\mathrm{die}})+G_1(1,t-\Delta)p_{G_1}F(1-p_{G_1}F^{\mathrm{die}}).$$

$$G_1(B,t)=G_1(B,t-\Delta)\left(1-p_{G_1}B^{\mathrm{out}}(1-p_{G_1}B^{\mathrm{die}})+p_{G_1}B\sum_{k=1}^{K_{G_1}}G_1(k,t-\Delta)D_{G_2}(k)(1-p_{G_1}F)(1-p_{G_1}^{\mathrm{die}}),\right.$$

$$G_1(Q,t)=\left\{\left[\left(G_2(B,t-\Delta)p_{G_2}B^{\mathrm{out}}+(1-p_{G_2}B^{\mathrm{in}})\sum_{k=1}^{K_{G_2}}G_2(k,t-\Delta)D_{G_2}(k)(1-p_{G_2}F)(1-p_{G_2}^{\mathrm{die}})\right)p_{\mathrm{mit}}bp_{G0}\right.\right.$$
$$\left.\left.+G_0(t-\Delta)p_{G0G1}(1-p_{G_0}^{\mathrm{die}})\right]p_{G_1}Q+G_1(Q,t-\Delta)\right\}(1-p_{G_1}Q^{\mathrm{die}}),$$

$$G_0(t)=G_0(t-\Delta)(1-p_{G0G1})(1-p_{G_0}^{\mathrm{die}})+\left[G_2(B,t-\Delta)p_{G_2}B^{\mathrm{out}}+(1-p_{G_2}B^{\mathrm{in}})\sum_{k=1}^{K_{G_2}}G_2(k,t-\Delta)D_{G_2}(k)\right.$$
$$\left.\times(1-p_{G_2}F)(1-p_{G_2}^{\mathrm{die}})\right]p_{\mathrm{mit}}(1-bp_{G0})(1-p_{G_0}Q),$$

$$G_0Q(t)=\left\{\left[G_2(B,t-\Delta)p_{G_2}B^{\mathrm{out}}+(1-p_{G_2}B^{\mathrm{in}})\sum_{k=1}^{K_{G_2}}G_2(k,t-\Delta)D_{G_2}(k)(1-p_{G_2}F)(1-p_{G_2}^{\mathrm{die}})\right]p_{mit}(1-bp_{G0})p_{G_0}Q\right.$$
$$\left.+G_0Q(t-\Delta)\right\}(1-p_{G_0}Q^{\mathrm{die}}).$$

(A1)

APPENDIX B: FITTING PROCEDURE

One of the main results of this work is that all three intermitotic phases are perturbed by cisplatin. Here we want to give an example of a particular fitting, with the aim of showing that if perturbations on a particular phase are not considered, the experimental data are not correctly reproduced. Let us consider a dose of 100 μM of cisplatin, and the recovery time 6–24 h. We assume that we have already fitted the recovery time 0–6 h, with the parameters reported in Figs. 8, 9, and 10. We recall that at 6 h we can make a comparison with the whole set of Anti-BrdUrd data, so that this initial set of parameters can be considered a good starting point. Our simulation, in good agreement with the experimental data, gives at 6-h, percentages of 68%, 19%, and 13% of cells in G_1, S, and G_2 phases, respectively, with a total number of cells (normalized, as usual, on 0-h control) of 0.64. At 24 h, the experimental data to fit are $\%G_1=35\%$, $\%S=39\%$, and $\%G_2=26\%$, while the total number of cells is 0.57. In this case, it is obvious that the parameters utilized for 0–6 h fit have to be changed, in order to fit 24-h data (when such evidence is not clear, a good starting point to fit a particular recovery time is to confirm the parameters utilized for the previous one): confirming the strong block in G_1, the experimental evidence of a sharp decrease in $\%G_1$ between 6 and 24 h could not be predicted by the simulation. Thus, as a first try, one can decide to act only on G_1 block parameters, decreasing its strength and allowing cell repair. As shown in Table V, even introducing low repairs (0.02) and reducing the block strength from 0.93 to 0.5, the G_1 percentages are raised. So one could think to raise the repair again and to reduce the block strength further, but this is not really the case: the total number of cells, indeed, is already too high, and the above described action would make it raise more. Thus, one may think about also introducing a G_2 block, confirming, as a first try, the value of 0.73 utilized for the 0–6-h recovery time. Now (see again Table V) the G_1 percentage, as well as the total number of cells (even if both are still too high), draw close to experimental values, but the G_2 percentage is strongly overestimated, while the S percentage is too poor. Lowering the G_2 block would again raise the G_1 percentage and the total number of cells, so that a better solution is to act on S freezing as well. Confirming the previous (0–6 h) value for this parameter, the solution is almost reached, and with a final refinement of the parameters (including a small S-cell loss), the fit results are good. In order to make our fitting procedure clear, and to show how it arises necessarily to perturb all three phases, we chose a particular dose and a particular recovery time. The whole set of experimental data has been fitted following the same procedure, always checking, in addition, that the complete kinetic scenario followed biological knowledge (as explained is Sec. IV).

TABLE V. 100 μM of cisplatin, for a recovery time of 24 h; experimental (Expt.) data compared with three different set of parameters. Sim.(1): only G_1 perturbation is considered, with a block strength of 0.5 and a 0.02 cell repair. Sim.(2): same as Sim.(1), with a G_2 block (strength: 0.73, no repair) in addition. Sim.(3): same as Sim.(2) with a 0.53 S freezing in addition. Sim.(3) already fits the experimental data well; with a small refinement of these parameters (owing to those reported in Figs. 8, 9, and 10) the fit becomes very satisfactory (as shown in Table II).

	$\%G_1$	$\%S$	$\%G_2$	N
Exp.	35	39	26	0.57
Sim.(1)	71	22	7	1.04
Sim.(2)	40	15	45	0.726
Sim.(3)	32	36	30	0.683

[1] H. M. Shapiro, *Practical Flow Cytometry*, 2nd ed. (Liss, New York, 1988).
[2] Y. Z. Chen, Yong-li Zhang, and E. W. Prohofsky, Phys. Rev. E **55**, 5843 (1997).
[3] P. C. Lorigan, T. Crosby, and R. E. Coleman, Drugs **51**, 571 (1996).
[4] J. Konopa, Biochemical Pharmacology **37** 2303 (1988).
[5] M. Jackel and P. Kopf-Maier, Cancer Chemother. Pharmacol. **27**, 464 (1991).
[6] A. Howard and S. R. Pelc, Exp. Cell Res. **2,** 178 (1951).
[7] A. Howard and S. R. Pelc, Heredity Suppl. **6**, 261 (1953).
[8] C. G. Steel, *Growth Kinetics of Tumors* (Clarendon, Oxford, 1977).
[9] P. Ubezio and A. Rossotti, Cell Tissue Kinet. **20**, 507 (1987).
[10] J. Hunter and J. Pines, Cell **79**, 573 (1994).
[11] L. H. Hertwell and M. B. Kastan, Science **266**, 1821 (1994).
[12] X. Grana and E. P. Reddy, Oncogene **11**, 211 (1995).
[13] J. E. Sisken and L. Morasca, J. Cell Biol. **25,** 179 (1965).
[14] P. Ubezio, Comput. Methods Programs Biomed. **31**, 255 (1990).
[15] J. W. Gray, F. Dolbeare, M. G. Pallavicini, and M. Vanderlaan, in *Techniques in Cell Cycle Analysis*, edited by J. W. Gray and Z. Darzynkiewicz (Humana, Clifton, NJ, 1987), pp. 93–137.
[16] H. A. Crissman and J. A. Steinkamp, in *Techniques in Cell Cycle Analysis* (Ref. [15]), pp. 163–205.
[17] P. Ubezio and A. Andreoni, Cytometry **6**, 109 (1985).
[18] P. Ubezio, Comput. Methods Programs Biomed. **19**, 159 (1985).
[19] P. Ubezio, G. Tagliabue, B. Schechter, and Z. Agur, Cancer Res. **54,** 6446 (1994).
[20] R. Martin and K. L. Teo, *Optimal Control of Drug Administration in Cancer Chemotherapy* (World Scientific, Singapore, 1994).